Modelling of transport phenomena in laser welding of dissimilar metals

G. Phanikumar and K. Chattopadhyay
Department of Metallurgy, Indian Institute of Science, Bangalore, India, and
Pradip Dutta
Department of Mechanical Engineering, Indian Institute of Science, Bangalore, India

Abstract *The transport phenomena (heat transfer, fluid flow and species distribution) are numerically modelled for the case of laser welding of dissimilar metals. The model involves convection in the weld pool along with melting and mixing. The associated metallurgical phenomenon is an extremely complex one, and the present work is a preliminary attempt to model the process after making suitable assumptions. The numerical study is performed using a pressure based finite volume technique after making appropriate modifications to the algorithm to include the associated phase change processes and dissimilarity in the metal properties. The phase change process is modelled using an enthalpy-porosity technique, while the dissimilar metal properties are handled using appropriate mixture theories. As a case study, we have used dissimilar couples of copper-nickel. It is observed that the weld pool shape becomes asymmetric even when the heat source is symmetrically applied on the two metals forming the couple. As the weld pool develops, the side melting earlier is found to experience more convection and better mixing. Corresponding experiments are performed using the same parameters as in the computations, showing a good qualitative agreement between the two results. A scale analysis is performed to predict the time scale of initiation of melting of each metal. The scale-analysis predictions show a good agreement with the numerical results.*

Nomenclature

C	= solutal weight fraction	*Greek symbols*		
C_{pl}	= specific heat in liquid state	α	= Thermal diffusivity	
D_{AB}	= solutal diffusivity	β_C	= coefficient of solutal	
H	= enthalpy		expansion	
k	= thermal conductivity	β_T	= coefficient of thermal	
L	= latent heat of fusion		expansion	
p	= pressure	η	= laser absorption efficiency	
Q	= laser power	μ	= viscosity	
$q''(r)$	= heat flux at top	ρ	= density	
r_q	= laser beam radius	σ_C	= solutal surface tension	
S_h, S_u, S_v, S_w	= source terms		coefficient	
T	= temperature	σ_T	= thermal surface tension	
T	= time		coefficient	
u, v, w	= velocities along x,y,z			

Introduction

Emerging technologies in various manufacturing applications now require dissimilar parts to be joined. Since physical properties of the two metals to be

joined can be very different from each other, it can lead to complexities in weld pool shape, solidification microstructure, segregation patterns, and formation of intermetallic compounds (Sun and Ion, 1995). Hence, from a scientific standpoint, analysis of a dissimilar metal joint offers a number of challenges. Although there exists a fairly large number of publications on the fusion joining of dissimilar metals, a review in the area shows that a majority of this literature is mainly concentrated on the joining of dissimilar steels and deal with the analysis of the problem in a case-by-case manner (Sun and Ion, 1995; Metzger and Lison, 1976). A systematic study from a scientific angle is therefore desirable in this field.

Mathematical modelling and simulation have been used to gain insight into the physical processes that occur in a weld pool (Chan *et al.*, 1984; Zacharia *et al.*, 1988; Dutta *et al.*, 1995; Debroy and David, 1995), as it is very difficult to make a direct observation of the weld pool solidification behaviour (Mohanty and Mazumder, 1998). Existing literature shows a good success in computer simulation of laser and arc welding of similar metals (Chan *et al.*, 1984; Zacharia *et al.*, 1988; Dutta *et al.*, 1995; Debroy and Davis, 1995), but very few studies on numerical simulation of dissimilar metal welding are reported. Recently, Chung and Wei (1999) performed a two-dimensional simulation of the molten pool of dissimilar metal welding using a volume-of-fluid technique. Dissimilar metal welding, however, is three-dimensional by nature even in a spot-welding mode due to the asymmetry created by the difference in properties of the two metals. In the present paper, we have made a preliminary attempt to perform a three-dimensional simulation of dissimilar welding for the first time. Because of the complexity in the process, it is necessary to make a few assumptions in the modelling work. The primary aim is to obtain a good insight for understanding the physical processes that take place in dissimilar welding.

A binary couple of pure metals is simpler to start with in order to understand the basic issues in dissimilar joints. In a model dissimilar couple, the two metals should have a significant difference in their physical properties so that the main issues are highlighted. Also, for a preliminary study, it is not desirable to choose a binary system with a phase diagram containing any miscibility gap or intermetallic compounds in it, which would make the system additionally complex and difficult for a systematic analysis. As shown in Table I, copper and nickel, indeed, have a large difference in thermophysical properties (Brandes, 1983). Also, the binary system of copper and nickel has a simple isomorphous phase diagram without any miscibility gap or intermetallic compounds. In this paper, we present a three-dimensional analysis of the transport phenomena occurring in dissimilar welds of copper and nickel in butt weld geometry.

Computational modelling
A full scale modelling of a moving dissimilar weld pool (i.e. produced by a continuous laser welding) requires modelling of the melting, mixing, and

Melting point (°C)	Cu	1,085	
	Ni	1,453	
Density (Kgm^{-3})	Cu	8,900	
	Ni	7,905	
Latent heat (kJmol^{-1})	Cu	13.02	
	Ni	17.16	
Thermal conductivity (Wm^{-1}K^{-1})	Cu	Solid: 279.5	
		Liquid: 170.7	
	Ni	Solid: 75	
		Liquid: 62	
Specific heat (JKg^{-1}K^{-1})	Cu	Solid: 440	
		Liquid: 484	
	Ni	Solid: 515	
		Liquid: 595	
Viscosity (Kgs^{-1}m^{-1})	Cu	2.85×10^{-3}	
	Ni	3.68×10^{-3}	
Surface tension coefficient (Nm^{-1}K^{-1})	Cu	-0.13×10^{-3}	
	Ni	-0.38×10^{-3}	

Table I.
Physical properties of
copper and nickel

solidification at both micro and macro scales. Solidification modelling in such a
situation is a very difficult task, since the composition can vary sharply at any
location. In addition, the solidification process would depend on the scale of
mixing of the two metals at the interface, which may be very difficult to
determine using present modelling tools. In the case of a stationary spot weld,
however, we can have a distinct process of melting during the application of the
laser, followed by a solidification process after the laser is switched off
(assuming there is no remelting). Since the melting process involves only pure
metals (initially separated in a butt welding arrangement), we have the option
to model it without having to consider the solidification process. It may be
noted that any mixing of metals due to convection occurs only after the
material is molten. In the present case we attempt to model the melting and
mixing processes at a macroscopic level by considering a stationary-welding
situation of a copper-nickel couple. The objective is to study the asymmetry of
a weld pool caused by a symmetric heat source on a dissimilar metal joint and
the associated temperature, velocity and mass fraction distributions. At this
point, one may note that dissimilar metal welding is inherently three-
dimensional even in a stationary spot-welding mode due to the asymmetry
created by the difference in properties of the two metals.

Choice of model
In the welding of dissimilar metals, the two metals melt and mix in the weld
pool. In order to model such a phenomenon, there are generally two
mathematical models that can be used for the flow of a multi-component fluid:

(1) locally homogeneous mixture model; and

(2) multi-fluid model.

In the flow of a multi-component mixture, if we assume that the various species are mixed at the atomic level and share the same velocity, pressure, and temperature fields, and that mass transfer takes place by convection and diffusion, then we can use a locally homogeneous model. The more complex situation where different species are mixed on larger scales, and may have separate flow fields, is called a "multi-phase" flow (Carver, 1984; Ishi and Mishima, 1984). The distinct flow fields of different fluids can interact via empirically specified "inter-phase transfer" terms (Ishi and Mishima, 1984). Simulation of such a flow would require a multi-fluid model, in which there is a separate solution field for each phase. Multi-fluid models rely on constitutive relations that are difficult to determine empirically.

For our simulation, we are considering a locally homogeneous model where flow is characterised by the properties assigned according to the relative proportion of each phase in the mixture. Correlations are required to provide estimates of properties in relevant flow regimes. Although some information regarding interface related quantities will be lost by assuming a locally homogeneous model, the present study may still give some insight into this complex problem with regard to flow field, asymmetry of pool shape, temperature field, and mixing.

Mathematical formulation
A schematic diagram of the computational domain used for numerical simulation is shown in Figure 1. Two pieces of copper and nickel with equal dimensions are kept in a butt joint. A laser heat input with a Gaussian distribution is applied from the top at the centreline of the butt joint such that the heat is distributed equally on both pieces. The following are the assumptions made in the model:

- The weld pool surface is flat.
- The fluid motion in the melt pool is assumed to be laminar and incompressible.
- The system is in unsteady state.
- Thermophysical properties are taken to be different for solid and liquid metals, and variation with temperature taken into consideration using a
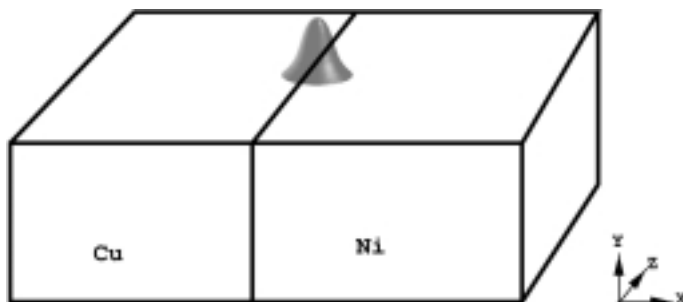
Figure 1.
Schematic of the
computational domain
with gaussian heat
source

smooth fit over the data available in the literature (Brandes, 1983). The physical properties also vary according to the concentration of the mixture, and are evaluated according to mixture theory. For properties of the mixtures, semi-empirical correlations are used. Thermal conductivity, specific heat, density, viscosity, and surface tension are considered as functions of temperature and mass fraction.

- Laser power is distributed in a Gaussian manner at the top surface. The coupling coefficient (laser power efficiency) remains constant.

The copper nickel system chosen is very close to an ideal binary system with complete miscibility in liquid and solid states, and hence it justifies most of the assumptions we have made with regard to our mixture model. One important property that is very difficult to estimate for the simulation is the efficiency of absorption of heat from the laser beam. While the surface finish and emissivity reduce the coupling efficiency, vapour and plasma formation on the surface of melt pool enhance the same. It is very difficult to get the coupling efficiency from experiments, and published literature on this issue is also not adequate. We have used an efficiency value close to what is generally found in the literature of laser welding of similar metals. In this context, it should be noted that the weld pool shape and qualitative details will be unaffected by small changes in the coupling efficiency and quantitative agreement with experimental results is not aimed at in this preliminary modelling attempt.

Phase change is modelled using an enthalpy-porosity technique (Brent *et al.*, 1988). As discussed earlier, only melting of pure metals need be considered if we are modelling the melting phenomenon in a stationary spot weld. For a given control volume, pure metal properties (including latent heat of fusion) are used until melting takes place. Once melting occurs, followed by transport of material from one zone to another and subsequent mixing of the two metals, mixture rules for the properties are applied. For this study, a linear variation of properties with mass fraction is assumed.

The resulting governing equations for mass, momentum, energy and species equations are as follows:

- *Continuity*:

$$\frac{\partial \rho}{\partial t} + \frac{\partial}{\partial x}(\rho u) + \frac{\partial}{\partial y}(\rho v) + \frac{\partial}{\partial z}(\rho w) = 0. \tag{1}$$

- *Momentum*:

$$
\begin{aligned}
&\frac{\partial}{\partial t}(\rho u) + \frac{\partial}{\partial x}(\rho u u) + \frac{\partial}{\partial y}(\rho v u) + \frac{\partial}{\partial z}(\rho w u) \\
&= \frac{\partial}{\partial x}\left(\mu \frac{\partial u}{\partial x}\right) + \frac{\partial}{\partial y}\left(\mu \frac{\partial u}{\partial y}\right) + \frac{\partial}{\partial z}\left(\mu \frac{\partial u}{\partial z}\right) - \frac{\partial p}{\partial x} + S_x
\end{aligned}
\tag{2}
$$

$$\frac{\partial}{\partial t}(\rho v) + \frac{\partial}{\partial x}(\rho uv) + \frac{\partial}{\partial y}(\rho vv) + \frac{\partial}{\partial z}(\rho wv)$$
$$= \frac{\partial}{\partial x}\left(\mu\frac{\partial v}{\partial x}\right) + \frac{\partial}{\partial y}\left(\mu\frac{\partial v}{\partial y}\right) + \frac{\partial}{\partial z}\left(\mu\frac{\partial v}{\partial z}\right) - \frac{\partial p}{\partial y} + S_y \tag{3}$$

$$\frac{\partial}{\partial t}(\rho w) + \frac{\partial}{\partial x}(\rho uw) + \frac{\partial}{\partial y}(\rho vw) + \frac{\partial}{\partial z}(\rho ww)$$
$$= \frac{\partial}{\partial x}\left(\mu\frac{\partial w}{\partial x}\right) + \frac{\partial}{\partial y}\left(\mu\frac{\partial w}{\partial y}\right) + \frac{\partial}{\partial z}\left(\mu\frac{\partial w}{\partial z}\right) - \frac{\partial p}{\partial z} + S_z. \tag{4}$$

- *Energy*:

$$\frac{\partial}{\partial t}(\rho H) + \frac{\partial}{\partial x}(\rho uH) + \frac{\partial}{\partial y}(\rho vH) + \frac{\partial}{\partial z}(\rho wH)$$
$$= \frac{\partial}{\partial x}\left(k\frac{\partial T}{\partial x}\right) + \frac{\partial}{\partial y}\left(k\frac{\partial T}{\partial y}\right) + \frac{\partial}{\partial z}\left(k\frac{\partial T}{\partial z}\right) + S_h. \tag{5}$$

- *Mass fraction*:

$$\frac{\partial C}{\partial t} + \frac{\partial}{\partial x}(uC) + \frac{\partial}{\partial y}(vC) + \frac{\partial}{\partial z}(wC)$$
$$= \frac{\partial}{\partial x}\left(D_{AB}\frac{\partial C}{\partial x}\right) + \frac{\partial}{\partial y}\left(D_{AB}\frac{\partial C}{\partial y}\right) + \frac{\partial}{\partial z}\left(D_{AB}\frac{\partial C}{\partial z}\right). \tag{6}$$

The above source terms according to our enthalpy-porosity formulation are expressed as follows:

$$S_x = -\left(\frac{K(1-\varepsilon)^2}{\varepsilon^3 + b}\right)u \tag{7}$$

$$S_y = -\left(\frac{K(1-\varepsilon)^2}{\varepsilon^3 + b}\right)v + \rho g[\beta_T(T - T_r) - \beta_C(C - C_r)] \tag{8}$$

$$S_z = -\left(\frac{K(1-\varepsilon)^2}{\varepsilon^3 + b}\right)w \tag{9}$$

$$S_h = -\frac{\partial}{\partial t}(\rho\Delta H), \tag{10}$$

where K is a morphological constant (a large number, say 10^8), b is an arbitrary small number to prevent division by zero, ΔH is the latent heat content of a control volume, and ε is the liquid fraction calculated as $\frac{\Delta H}{L}$, with L being the latent heat of melting for the corresponding metal. The enthalpy, H, used in equation (5) is defined in the liquid state at any location using mixture theory, as follows:

$$H_{mix} = H_{Cu}C + H_{Ni}(1 - C), \tag{11}$$

where H_{Cu} and H_{Ni} are the enthalpies of copper and nickel, respectively, at a given temperature. The first terms in each of the equations (7)-(9) represent the porous medium-like resistance in the mushy region at the solid-liquid interface. In the fully liquid region, the value of ε is 1, making the porous medium resistance terms zero. On the other hand, in the fully solid region, $\varepsilon = 0$, thus forcing the porous medium resistance terms in equations (7)-(9) to be very large. This large source term offers a high flow resistance, making the velocities in the entire solid region effectively zero. In the mushy region, however, ε lies between 0 and 1, and the porous medium resistance varies smoothly from zero in the liquid region to a high value in the solid region, thus making the velocities vary accordingly.

Boundary and initial conditions: At time $t = 0$, the entire domain is in the solid state at room temperature. At time $t > 0$, the following boundary conditions are applied.

At the top surface of the workpiece, a heat flux with a Gaussian distribution is applied, as given by:

$$q''(r) = \frac{\eta Q}{\pi r_q^2} \exp\left(-\frac{r^2}{r_q^2}\right). \tag{12}$$

At the flat free surface of the liquid, shear force due to surface tension (Marangoni force) is expressed as:

$$\mu \frac{\partial u}{\partial y}\bigg|_{y=h} = \sigma_T \frac{\partial T}{\partial x}\bigg|_{y=h} + \sigma_C \frac{\partial C}{\partial x}\bigg|_{y=h} \tag{13}$$

$$\mu \frac{\partial w}{\partial y}\bigg|_{y=h} = \sigma_T \frac{\partial T}{\partial z}\bigg|_{y=h} + \sigma_C \frac{\partial C}{\partial z}\bigg|_{y=h}. \tag{14}$$

Also, no mass transfer is considered at the top surface. The bottom surface is insulated, while the four sides are subjected to convective and radiative heat loss.

As shown in equations (13) and (14), the Marangoni force is balanced by viscous shear force at the top surface. Since fluid is pulled in the direction of increasing surface tension, a negative surface tension coefficient would result in a surface flow away from the laser centre towards the pool edges. The

thermal Marangoni number (based on temperature gradient) for this problem can be defined as:

$$Ma = \frac{\sigma_T L r_q}{\alpha C_{pl} \mu}. \tag{15}$$

Since we are using variable properties in this paper, the governing equations are not non-dimensionalised with Marangoni number, which is not a fixed quantity for the problem. Representative values of Marangoni number for the copper and nickel at 1,600°C are 625 and 3,863, respectively.

Numerical procedure
The three-dimensional coupled continuity, momentum, energy, and mass fraction equations along with the boundary conditions are solved numerically using a finite volume technique. The general framework of the numerical solution rests on SIMPLER algorithm (Patankar, 1980), modified appropriately to accommodate phase change processes and mixing of dissimilar metals. Transient studies are carried out till some mixing patterns are obtained. The average values of thermophysical data are listed in Table I, and the process parameters used for the case study are given in Table II. A non-uniform grid of $64 \times 48 \times 64$ is used to discretise the computational domain, with a high concentration of grids inside the weld pool.

The time steps for computations are varied according to the stages of the melting process. During the conduction phase, large time steps (about 0.25ms) may be allowed until melting begins (typically after 0.5ms). Once melting starts, the large temperature gradients in the melt pool set up a strong Marangoni convection, leading to very high fluid velocities, typically O(1m/s). Hence, time steps during the initial stages of pool development are chosen to be very small (about 0.05ms). Also, the relaxation factor for updating the enthalpy source term must be kept low (about 0.1) to avoid numerical oscillations. The other relaxation factors used for the iterations are 0.3 for the three momentum equations, 0.4 for the mass fraction equation and 0.9 for the energy equation.

Results and discussion
Owing to the difference in thermal diffusivity of copper and nickel, heat diffusion in copper will be more during the conduction phase of the heating process. Nickel, which has a lower thermal conductivity, will experience a faster temperature rise than copper. As a result, the location of maximum temperature will be shifted towards the nickel side. Depending on the rate of heating of the two metals and their respective melting points, we can expect

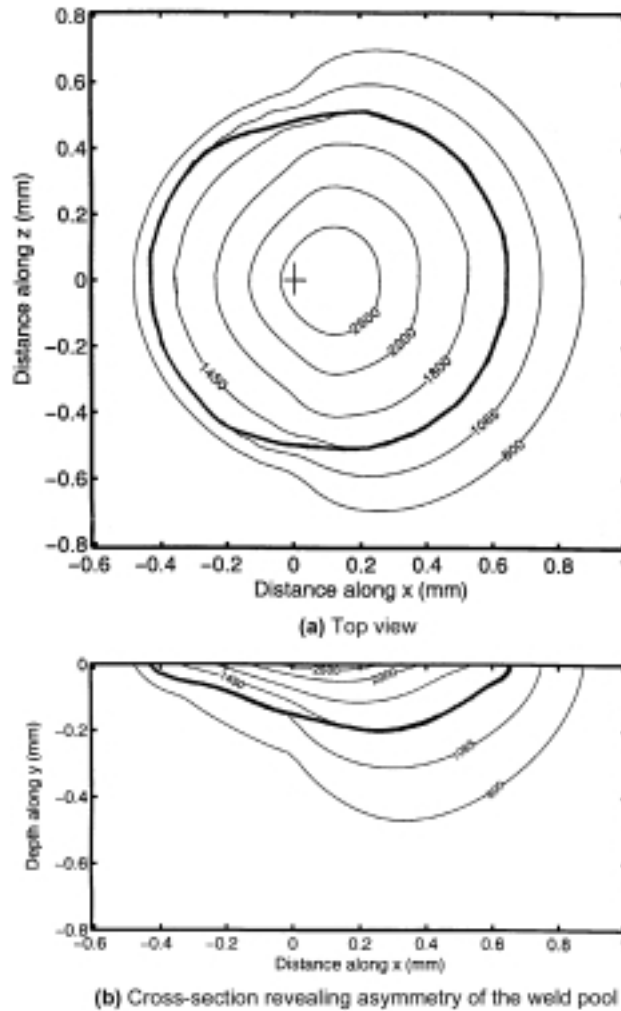|	
Power of the laser	2,500W
Diameter of the beam	0.5mm
Efficiency of heat input	0.3
Work piece dimensions	12mm × 10mm × 12mm

Table II.
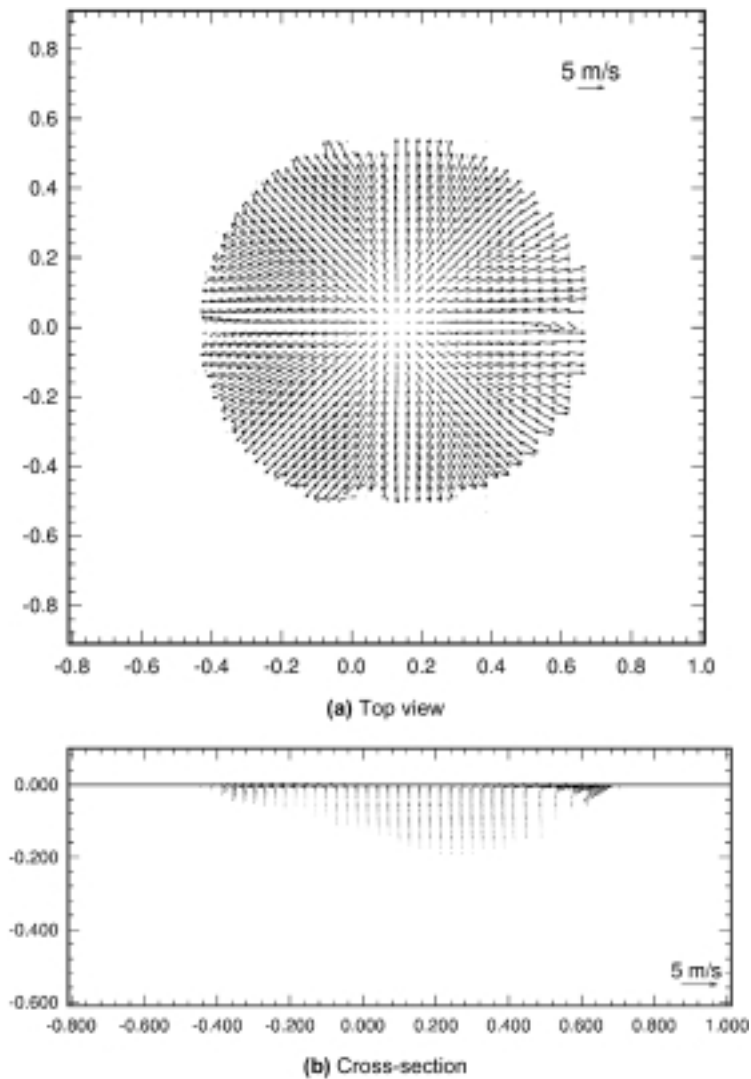Process parameters
used in the simulation

either of the two metals to melt first. In the present case, the low thermal conductivity of nickel more than compensates for its high melting point and it melts first.

After nickel starts melting, the weld pool develops a flow starting from the maximum temperature location and moves outwards. Since the temperature coefficient of the surface tension, σ_T, is negative, the value of the surface tension at the maximum temperature location is lower than that at the edges of the weld pool. Hence, the fluid in the centre is pulled radically outward. From Figures 2 and 3 it can be seen that due to asymmetric heating and convection, isotherms bend and become non-circular. On the free surface, convection brings the hot liquid from the maximum temperature location to the edges of the weld

(a) Top view

(b) Cross-section revealing asymmetry of the weld pool

Note: Laser is centered at (0,0,0). The temperatures are in °C.

Figure 2.
Calculated temperature contours in the weldpool after 0.5s revealing asymmetry of the weld pool

pool, thus increasing the width of the weld pool. By continuity, this flow also
brings the cold fluid from the bottom of the pool to the surface. The amount of
heat transported in the vertical direction is therefore relatively small. Hence, the
melt pool tends to be shallow and wide. Since surface tension forces are
dominant, the maximum velocity occurs on the free surface. The eye of the
convection cell is close to the surface. The corresponding composition
distributions on the pool surface and at some depth below the pool surface are
shown in Figures 4a and 4b, respectively. Both figures indicate that there is
better mixing on the nickel side, which also experiences more vigorous

convection. Also, on comparing Figures 4a and 4b, it may be observed that mixing is better on the pool surface, where convection is stronger.

Figure 5 shows a top view of the evolution of heating and weld pool formation. It is observed that the nickel side melts first, and subsequently convection carries the heat towards the copper side. Thus, the rise in temperature and melting of the copper side is aided by convection from the nickel side, in addition to direct laser heating. This information is not easily obtainable from experiments alone, and hence it is considered to be an important contribution from our numerical modelling. The final melt pool shape is determined by the convection patterns, which results in an asymmetric weld pool as also observed in experiments (Chung and Wei, 1999). In this

(a) Top view

(b) Horizontal section at a depth of 0.1mm
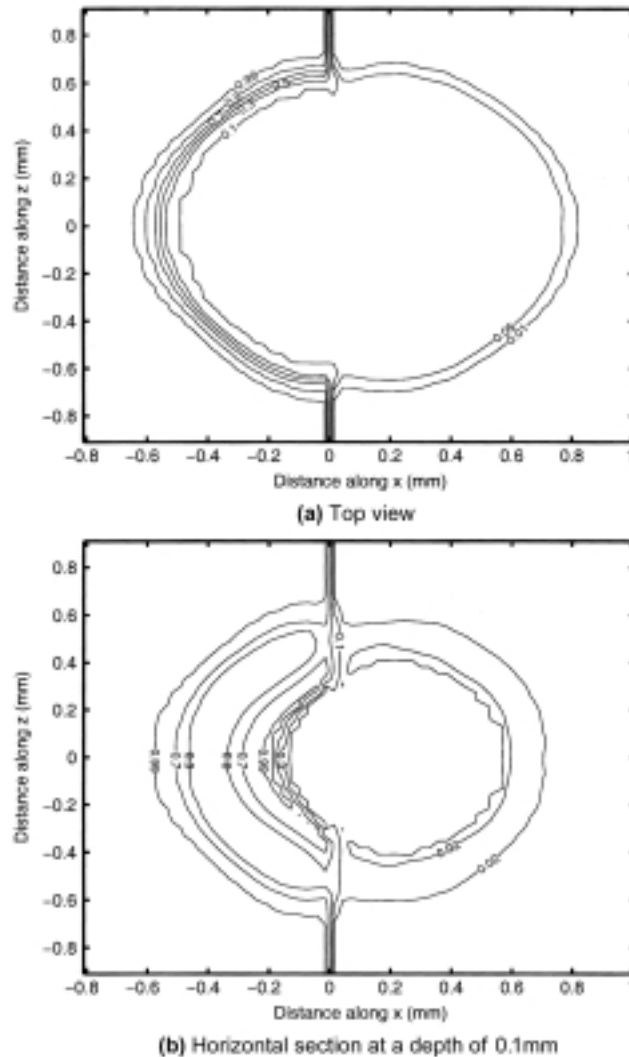
Figure 4.
Calculated composition contours showing composition distribution of copper after 0.5s
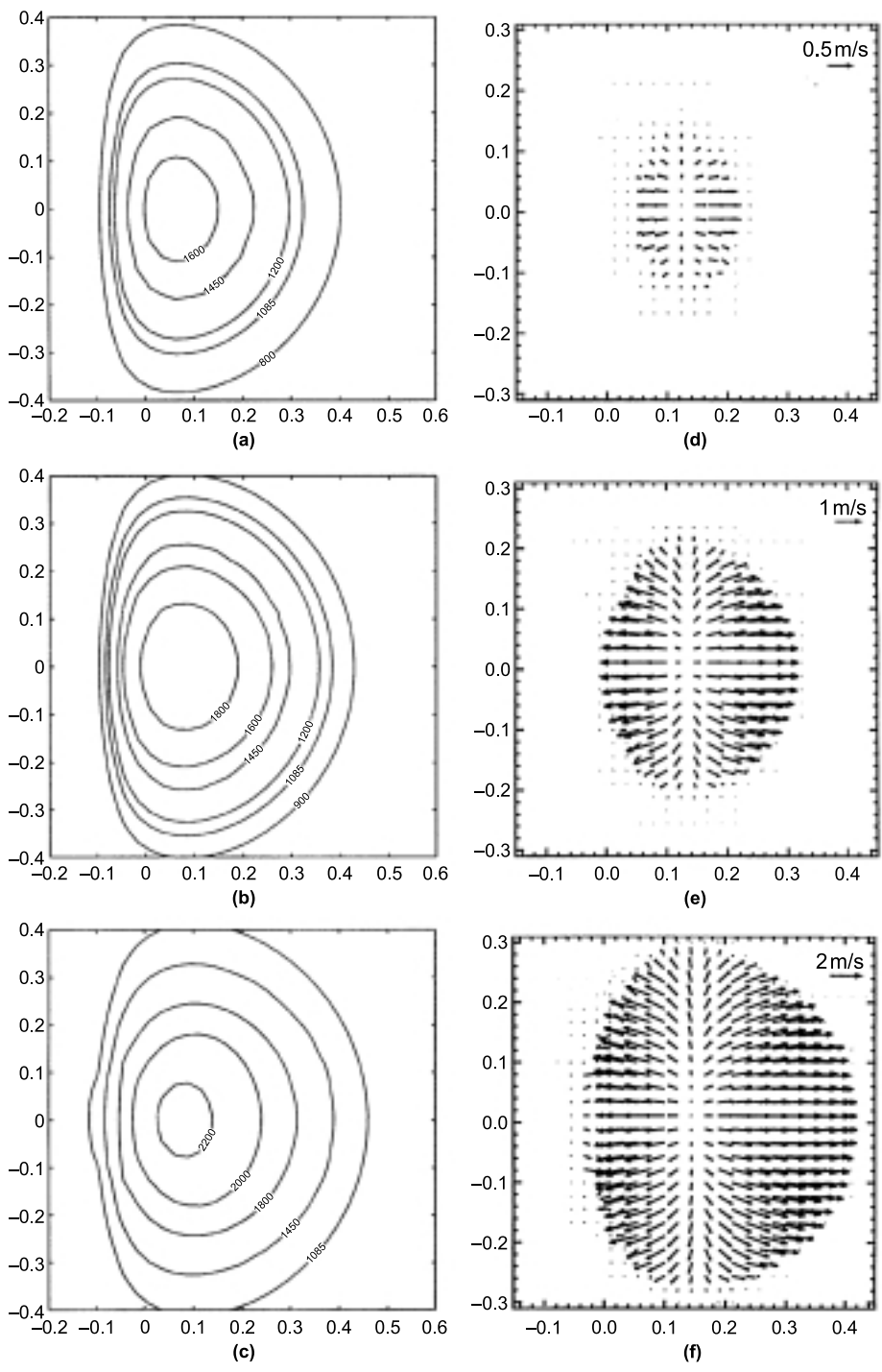
Figure 5.
Evolution of weld pool
(top view). Temperature
contours at (a) 2ms;
(b) 5ms; (c) 20ms.
Velocity profiles at
(d) 2ms; (e) 5ms; (f) 20ms

simulation, we have used the same value of efficiency of laser absorption for both the metals, and hence the observed asymmetry in the melt pool is entirely due to the difference in thermal transport properties of the two metals. We have also run simulations using differential laser absorption efficiencies for the two metals, but the effect is found to be less significant.

For the purpose of qualitative validation of our model, we have made some comparisons with corresponding experimental studies. Since the present computational studies have been performed for the case of stationary spot welding, corresponding stationary welding experiments have also been performed. This is shown in Figure 6, and the qualitative agreement of the weld pool shift is found to be good. Variation of mass fraction of nickel across the weld pool on the top surface has been computed and plotted as shown in Figure 7b. This agrees well with the corresponding experimental results shown in Figure 7a. The agreement is a qualitative one, showing the general trend of composition variation. However, the composition curve obtained from computation appears to be smoother, which can be attributed to the assumption of local homogeneity in our mixture model.

Scale analysis
We have observed in the previous section that nickel melts before copper does, although the former has a higher melting point. A possible cause identified for this phenomenon is the higher thermal conductivity of copper. There are several other properties such as density, specific heat, and latent heat, each of which could also play a role in determining the time for initiation of melting after the laser is switched on. In this section, a systematic scale analysis is
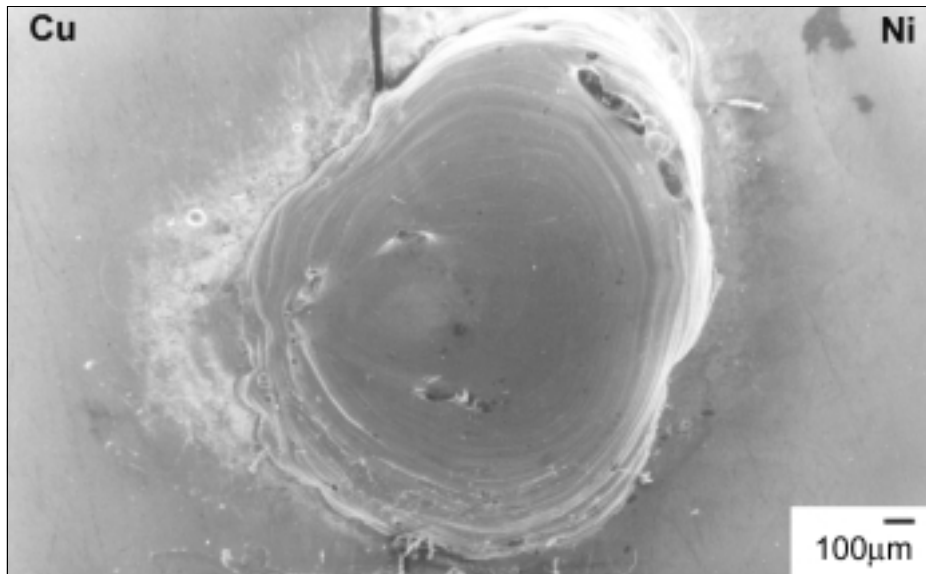
Figure 6.
Secondary electron image of top view of a Cu-Ni spot weld with the same parameters as used in the simulation
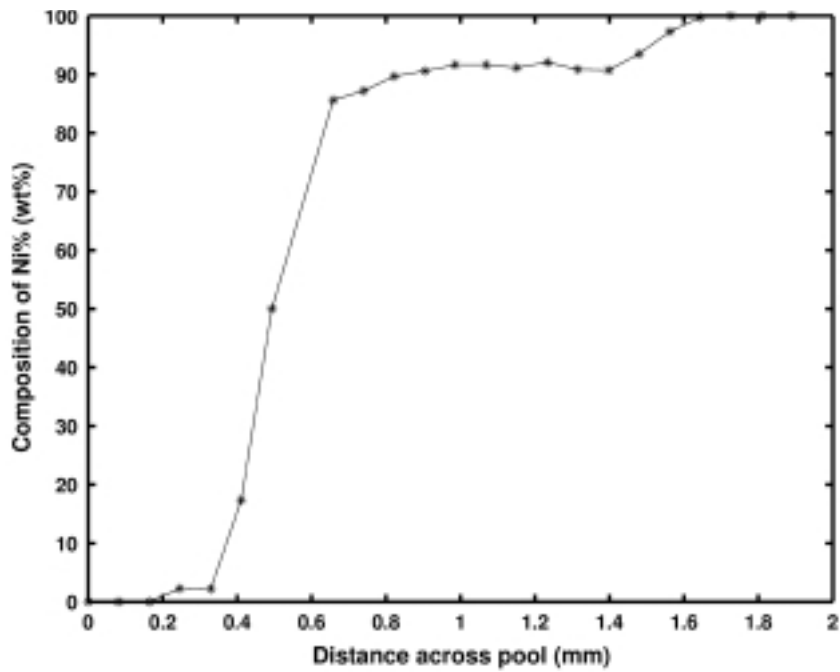
(a) experimental (EDAX)
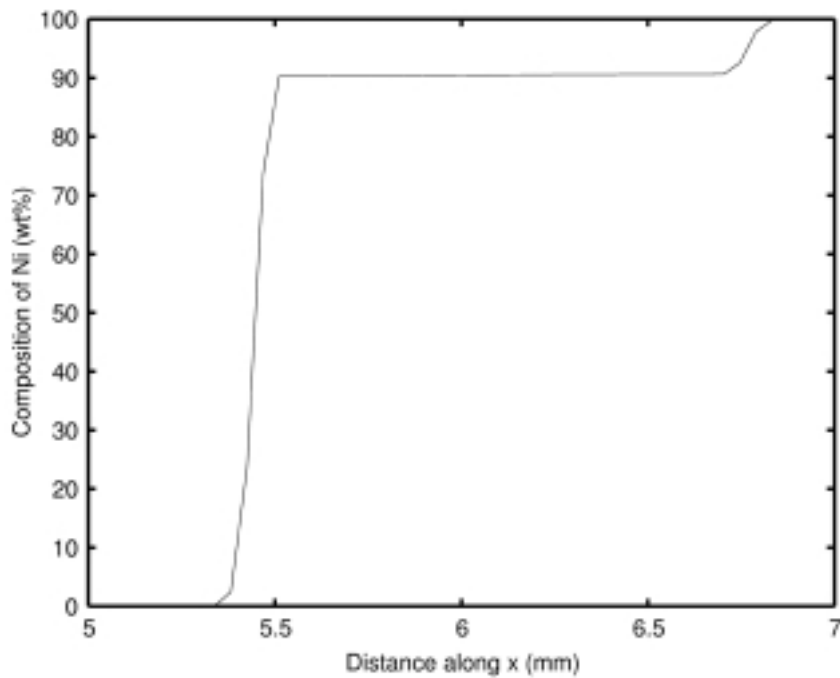
(b) computational

Figure 7.
Composition of nickel
(wt %) across the weld
pool

performed, from which we may be able to predict time scales for initiation of melting of each metal in a dissimilar couple.

Before melting occurs, the mode of energy transport is pure conduction. Accordingly, the energy equation (5) takes the following form in this regime:

$$\frac{\partial}{\partial t}(\rho cT) = \frac{\partial}{\partial x}\left(k\frac{\partial T}{\partial x}\right) + \frac{\partial}{\partial y}\left(k\frac{\partial T}{\partial y}\right) + \frac{\partial}{\partial z}\left(k\frac{\partial T}{\partial z}\right). \tag{15}$$

The diffusion terms on the right-hand side of equation (15) are all of the same order of magnitude. Let us consider only the term $\frac{\partial}{\partial y}\left(k\frac{\partial T}{\partial y}\right)$. The transient heating term on the left side of equation (15) should also be of the same order of magnitude. In other words,

$$\frac{\partial}{\partial t}(\rho cT) \sim \frac{\partial}{\partial y}\left(k\frac{\partial T}{\partial y}\right). \tag{16}$$

We define a length scale, y_{ref}, representing the penetration of heat by diffusion as a result of the laser heat flux acting on the top of the workpiece. With this definition, the rate of energy absorption per unit volume can also be scaled as $\frac{q}{y_{ref}}$. Hence, one can write:

$$\frac{\partial}{\partial t}(\rho cT) \sim \frac{\partial}{\partial y}\left(k\frac{\partial T}{\partial y}\right) \sim \frac{q}{y_{ref}}. \tag{17}$$

When melting initiates, the temperature at the top surface is T_m, while the temperature at a distance y_{ref} from the top surface will be nearly that of ambient (since y_{ref} represents a diffusion length scale). Defining $\Delta T = T_m - T_{ambient}$, one can rewrite equation (17) as:

$$\frac{\rho c\Delta T}{t_{ref}} \sim \frac{k\Delta T}{(y_{ref})^2} \sim \frac{q}{y_{ref}}, \tag{18}$$

where t_{ref} is the time scale for initiation of melting. Eliminating y_{ref} from the above equation, we get:

$$t_{ref} \sim \rho ck(\tfrac{\Delta T}{q})^2. \tag{19}$$

The above expression suggests that, for the same laser heat flux, q, the time for initiation increases with density, specific heat, thermal conductivity, and the melting temperature of the particular material. Substituting the average property values of copper and nickel into the above expression and using an average laser intensity, it is found that $(t_{ref})_{nickel} \sim 0.2$ms and $(t_{ref})_{copper} \sim 0.4$ms. The numerical results, too, predict an early melting of nickel compared to copper.

Conclusions

Laser welding of dissimilar materials consisting of a copper-nickel couple has been studied numerically. In spite of some simplifying assumptions, the model is able to capture some of the key features of the process such as differential heating of the two metals, asymmetric weld pool development, and mixing of molten metals. The computational results show a good qualitative agreement with the corresponding experimental ones. A scale analysis is also performed for predicting the time required for initiation of melting of a metal, and the agreement with numerical results is found to be excellent. This work lays a strong foundation for future studies of some of the complex issues in dissimilar joints.

References

Brandes, F.A. (1983), *Smithells Metals Reference Book*, 6th ed., Butterworths & Co. Publications, London.

Brent, A.D., Voller, V.R. and Reid, K.J. (1998), "The enthalpy porosity technique for modelling convection-diffusion phase change: application to the melting of a pure metal", *Numerical Heat Transfer*, Vol. 13, pp. 297-318.

Carver, M.B. (1984), "Numerical computation of phase separation in two fluid flow", *Journal of Fluid Engineering*, Vol. 106, pp. 147-53.

Chan, C.L., Mazumder, J. and Chen, M.M. (1984), "A two-dimensional transient model for convection in laser melted pool", *Metallurgical Transactions*, Vol. 15A, pp. 2175-84.

Chung, F.F. and Wei, P.S. (1999), "Mass, momentum, and energy transport in a molten pool when welding dissimilar metals", *Journal of Heat Transfer*, Vol. 121, pp. 451-61.

Debroy, T. and David, S.A. (1995), "Physical processes in fusion welding", *Reviews of Modern Physics*, Vol. 67 No. 1, pp. 85-112.

Dutta, P., Joshi, Y. and Janaswamy, R. (1995), "Thermal modelling of arc welding processes with non-axisymmetric boundary conditions", *Numerical Heat Transfer*, Part A No. 27, pp. 499-518.

Ishii, M. and Mishima, K. (1984), "Two-fluid model and hydrodynamic constitutive relations", *Nuclear Engineering and Design*, Vol. 82, pp. 107-26.

Metzger, G. and Lison, R. (1979), "Electron beam welding of dissimilar metals", *Welding Journal*, Vol. 55 No. 8, pp. 230s-40s.

Mohanty, P.S. and Mazumder, J. (1998), "Solidification behaviour and microstructural evolution during laser beam-material interaction", *Metallurgical Transactions*, Vol. 29B, pp. 1269-79.

Patankar, S.V. (1980), *Numerical Heat Transfer and Fluid Flow*, Hemisphere Publications, New York, NY.

Sun and Ion, J.C. (1995), "Laser welding of dissimilar metal combinations", *Journal of Materials Science*, Vol. 30, pp. 4205-14.

Zacharia, T., Eraslan, A.H. and Aidun, D.K. (1988), "Modelling of autogenous welding", *Welding Journal*, Vol. 67, pp. 53s-62s.